Letter Vol. 48, No. 2 / 15 January 2023 / Optics Letters 211

Simulated wrapped phase optimizes phase retrieval in phase-shifting interferometry

Xindong Zhu,[1,†] Liping Lian,[2,†] Pengcheng Yang,[2] Zehong Chang,[1] Xiaoting Huang,[1] Xian Wang,[3] Zijian Yu,[2] and Pei Zhang[1,4,*]

[1]Ministry of Education Key Laboratory for Nonequilibrium Synthesis and Modulation of Condensed Matter, Shaanxi Province Key Laboratory of Quantum Information and Quantum Optoelectronic Devices, School of Physics, Xi'an Jiaotong University, Xi'an 710049, China
[2]Mechanical and Electrical Engineering College, Xi'an Polytechnic University, Xi'an 710048, China
[3]School of Mechanical and Precision Instrument Engineering, Xi'an University of Technology, Xi'an 710048, China
[4]State Key Laboratory of Applied Optics, Changchun Institute of Optics, Fine Mechanics and Physics, Chinese Academy of Sciences, Changchun 130033, China
*Corresponding author: zhangpei@mail.ustc.edu.cn
†These authors contributed equally to this work.

Received 27 September 2022; revised 15 November 2022; accepted 28 November 2022; posted 1 December 2022; published 2 January 2023

Phase retrieval is crucial in phase-shifting interferometry and other phase measurement techniques. However, in noisy wrapped phase maps with high steepness, discontinuities arise and cause phase unwrapping errors. To solve this problem, this Letter presents a phase retrieval method based on a simulated wrapped phase. By establishing the correspondence between the simulated and measured interferograms, the difference in wrapped phases between them can be obtained. The difference in wrapped phase map, which has sparse and wide interference fringes, has a higher reliability of phase unwrapping. The proposed method not only possesses high phase retrieval accuracy but it also simplifies the processing of interferograms. Furthermore, the layout of all interferometric systems, the parameters of optical components, and the model of the measured object are known, so the proposed method can be used as a reference for phase retrieval.

https://doi.org/10.1364/OL.476543

Phase-shifting interferometry [1], which has the advantages being fast and non-contact and having high precision and resolution and a well-defined traceability to the definition of meter [2], is widely used for measuring displacement [3,4], detecting optical elements [5,6], measuring the surface deformation of objects [7,8], etc.

Phase retrieval [9] is a wavefront-sensing method that uses a series of intensity measurements to reconstruct the wavefront [5]. Phase retrieval, which determines the accuracy and even the reliability of measurement results, is crucial in phase-shifting interferometry. Phase retrieval often includes two processes: calculating the wrapped phase and phase unwrapping. In general, the principal (wrapped) phase is often calculated with the arctangent and the values are restricted to the interval $(-\pi, \pi]$. 2D phase unwrapping is used to restore the true phase values using the assumption that the unwrapped phase map is a continuous surface.

In high-reliability wrapped maps, correct phase unwrapping is easy to implement. However, in noisy wrapped phase maps with high steepness, discontinuities arise when the fringes are not sampled at a sufficiently high spatial frequency or the surface to be measured contains holes or cracks. These discontinuity sources can easily cause phase unwrapping errors. Existing research has mainly focused on the process of phase unwrapping, and many effective unwrapping methods have been proposed. These methods can be grouped into four major categories [10]: path-following methods [11–13] have high accuracy, a slow speed, and error diffusion; minimum-norm methods [14–17] are fast, but sometimes the precision is not very high; filtering-based methods [18–21] do both the phase unwrapping and filtering at the same time, but the algorithms are relatively complex and the speeds are relatively low; and deep-learning-based methods [22–25] have an overwhelming robustness, but they require a large amount of data to train the models, which are complex.

The reliability of wrapped phases is the basis of and key to phase retrieval. Simply improving the unwrapping algorithm is only a common way to obtain satisfactory results. Another way to obtain better unwrapping results is to enhance the reliability of the wrapped phases. As far as we know, there is no research on obtaining high-reliability wrapped phases with sparse interference fringes by using a simulated phase.

In this Letter, we introduce the use of a simulated wrapped phase in phase retrieval. By establishing pixel-level correspondence between the simulated and measured interferograms, the difference in wrapped phase between them can be obtained. There are two advantages for calculating the difference in wrapped phases. First, the reliability of the unwrapped phase is enhanced. On the one hand, the fewer the fringe number, the simpler the unwrapping process and the higher the reliability. The simulated and the measured phases are relatively similar, and the subtraction phase difference between them are small; thus, the fringe number of the whole wrapped-phase map is decreased. On the other hand, the processing accuracy is proportional to the width of the interference fringe [26]. The fringes become wider after subtraction (the essence of this phenomenon

is that the measured interferogram contains shape error while the simulated interferogram does not; the wide fringes after subtraction mainly refer to the shape error), and the accuracy of phase unwrapping is improved. Second, simulated phases are often used as measurement data in the relevant comparative measurement processes [27], the relative phase information (shape error) for the measured surface can be directly obtained, and the interferogram's processing flow is simplified.

The proposed method mainly includes the following four steps:

(1) According to the parameters of the measured surface, the simulated interferogram and wrapped phases can be obtained by ray tracing.
(2) The relationship between the simulated interferogram and the collected interferogram is established by image matching algorithms.
(3) The difference between the measured phase value and the simulated phase value is calculated. A new wrapped phase map can be harvested. Because the new wrapped phase changes slowly, the fringe density decreases significantly, which improves the reliability of phase unwrapping.
(4) Phase unwrapping. The existing 2D phase-unwrapping method is adopted to calculate the unwrapped phase.

Each step is now described in detail in the following.

Simulate the interferogram and wrapped phase of the measured surface. The theoretical model (equation) of the measured surface is known. First, the measured surface is discretized uniformly into $(\mathrm{H}+1)\times(\mathrm{W}+1)$ grid points along the height and width directions, where H and W are positive integers. Any grid point is denoted as $\mathrm{G}(h, w)$ where $h = 0, 1, \ldots,$ H and $w = 0, 1, \ldots,$ W. The parameters of the interferometer are known. Then, with a ray-tracing method, every grid point is traced to get a corresponding image point on the detector, and all the image points form the profile of an interferogram. Last, for every image point, we calculate the optical path difference between two optical paths and transform it into a phase difference. After the ray tracing has been put into practice for all grid points, an accurately simulated interferogram can be obtained. The optical path difference of any point $\mathrm{G}(h, w)$ on the measured surface can be denoted as

$$\begin{cases} \Delta L_{\mathrm{O}}(h, w) = L_{\mathrm{O}}(h, w) - L_{\mathrm{Omin}} \\ \Delta L_{\mathrm{R}}(h, w) = L_{\mathrm{R}}(h, w) - L_{\mathrm{Rmin}}, \end{cases} \tag{1}$$

where $\Delta L_{\mathrm{O}}(h, w)$ and $L_{\mathrm{O}}(h, w)$ are the relative and traced optical path differences in the object path; L_{Omin} is the minimum of $L_{\mathrm{O}}(h, w)$. $\Delta L_{\mathrm{R}}(h, w)$ and $L_{\mathrm{R}}(h, w)$ are the relative and traced optical path differences in the reference path; L_{Rmin} is the minimum of $L_{\mathrm{R}}(h, w)$. The relative optical path differences of the object arm and the reference arm can be calculated as

$$\Delta L_s(h, w) = \Delta L_{\mathrm{O}}(h, w) - \Delta L_{\mathrm{R}}(h, w). \tag{2}$$

Reference [28] takes the gear-tooth surface as the real object and puts forward a method of simulating the interferogram. The wrapped phase can be expressed as

$$\Delta\varphi_s(h, w) = \frac{2\pi}{\lambda} \times \left(\frac{\Delta L_s(h, w)}{\lambda} - \left\langle \frac{\Delta L_s(h, w)}{\lambda} \right\rangle - \frac{\lambda}{2}\right), \tag{3}$$

where $\langle\rangle$ is the symbol for rounding, and λ is the wavelength of the laser.

Match the simulated interferogram and the captured interferogram. As the conditions of the actual measurement and the simulation calculation are different, the scale and rotation angle between the captured interferogram and the simulated interferogram are inconsistent. In order to establish a point-to-point mapping relationship between the simulated and measured interferograms, it is necessary to match the interferograms. The boundaries of the measured interferogram are used as a reference while changing the coordinates of the simulated points on the simulated interferogram to make the simulated and measured interferograms match. In this research, we found that a rigid matching method should be adopted. If (x, y) is the coordinate of a simulated point after matching and (x_0, y_0) is the coordinate of a simulated point before matching, the mathematical model of the matching process is as follows:

$$\begin{pmatrix} x \\ y \end{pmatrix} = s \cdot \begin{pmatrix} \cos\theta & -\sin\theta \\ \sin\theta & \cos\theta \end{pmatrix} \cdot \begin{pmatrix} x_0 \\ y_0 \end{pmatrix} + \begin{pmatrix} t_x \\ t_y \end{pmatrix}, \tag{4}$$

where s is the zoom factor; θ is the rotation angle; $(t_x, t_y)^{\mathrm{T}}$ is the translation amount. The iterative closest point with bounded scale (ICPBS) algorithm [29] is used to precisely obtain the optimal values of s, θ, and $(t_x, t_y)^{\mathrm{T}}$. The minimization of the sum of the squares of the distances between the simulated and measured feature point sets is used to evaluate how good the matching is. Reference [29] gives more details about the ICPBS algorithm and how to obtain the optimal values of s, θ, and $(t_x, t_y)^{\mathrm{T}}$.

Calculate the difference between the measured and the simulated phase values. The measured wrapped-phase value $\Delta\varphi_m(h, w)$ can be calculated by

$$\Delta\varphi_m(h, w) = -\arctan \frac{\sum_{i=1}^{N} I_{mi}(h, w)\sin\delta_i}{\sum_{i=1}^{N} I_{mi}(h, w)\cos\delta_i}, \tag{5}$$

where $I_{mi}(h, w)$ is the intensity of pixel (h, w) on the ith interferogram. δ_i with $i = 0, 1, \ldots, \mathrm{N}-1$ is the phase step generated to obtain N interferograms; an $\mathrm{N}\times 3$ system is then formed that can be solved when $N \geq 3$. The simulated wrapped phase $\Delta\varphi_s(h, w)$ can be calculated by Eq. (3). The difference between the measured and the simulated phases can be written as

$$\Delta\varphi(h, w) = |\Delta\varphi_m(h, w) - \Delta\varphi_s(h, w)| - \pi. \tag{6}$$

Phase unwrapping. The fringe density becomes sparse upon subtracting the simulated wrapped phases from the measured ones. The difficulty of phase unwrapping is reduced, and the accuracy is improved. The existing 2D phase-unwrapping method is adopted to calculate the unwrapped phase.

Some experiments have been carried out to prove the correctness of the proposed phase retrieval method. A set of interferograms of a gear-tooth flank are captured based on a modified Mach–Zehnder interferometer. The interferometer is introduced in [30]. The first frame of the captured interferograms is shown in Fig. 1(a). The wrapped phase map of the interferograms can be calculated by Eq. (5). The result is shown in Fig. 1(c).

The simulation method for a gear-tooth flank's interferogram is introduced in [28]. The simulated interferogram is shown in Fig. 1(b); the simulated wrapped-phase map is generated by Eq. (3) and the results are shown in Fig. 1(d). Then, the

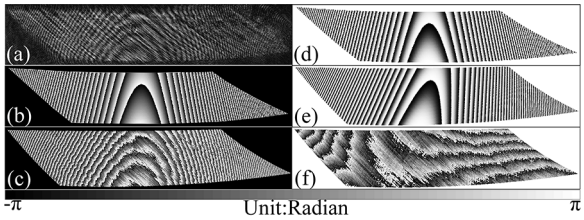

Fig. 1. Interferograms and processing: (a) interferogram; (b) wrapped phase map; (c) simulated interferogram; (d) simulated wrapped phase map before matching; (e) simulated wrapped phase map after matching; (f) wrapped phase map after subtraction.

introduced matching method is used to ensure correspondence between the simulated and measured interferograms. The simulated wrapped-phase map after matching is shown in Fig. 1(e). Based on Eq. (6), the difference in wrapped phase map is shown in Fig. 1(f). Comparing Figs. 1(c) and 1(f), we find that the density of fringes is significantly decreased. With the help of the proposed method, the wrapped phase map with dense fringes can be transformed into a wrapped phase map with sparse fringes.

The pseudocorrelation (PSD) and phase derivative variance (PDV) values were calculated to evaluate the phase reliability in [26], and are proportional to the phase reliability. The PSD and PDV values can be expressed as

$$\begin{cases} PSD(x,y) = \frac{1}{k^2}\sqrt{\left(\sum_{i=x-k/2}^{x+k/2}\sum_{j=y-k/2}^{y+k/2}\cos\varphi_{i,j}\right)^2 + \left(\sum_{i=x-k/2}^{x+k/2}\sum_{j=y-k/2}^{y+k/2}\sin\varphi_{i,j}\right)^2} \\ PDV(x,y) = -\frac{1}{k^2}\left(\sqrt{\sum_{i=x-k/2}^{x+k/2}\sum_{j=y-k/2}^{y+k/2}\left(\Delta_{i,j}^{x}-\overline{\Delta_{k,k}^{x}}\right)^2} + \sqrt{\sum_{i=x-k/2}^{x+k/2}\sum_{j=y-k/2}^{y+k/2}\left(\Delta_{i,j}^{y}-\overline{\Delta_{k,k}^{y}}\right)^2}\right), \end{cases} \tag{7}$$

where $\varphi_{i,j}$ is the wrapped phase at coordinate (i,j) of the wrapped phase map; k is the size of a kernel matrix whose center point is (x,y); $\Delta_{i,j}^{x}$ and $\Delta_{i,j}^{y}$ are the partial derivatives of the wrapped phase in the x and y directions, respectively; and $\overline{\Delta_{k,k}^{x}}$ and $\overline{\Delta_{k,k}^{y}}$ are the average values in the $k \times k$ window. The PSD and PDV values of the captured interferograms should be as large as possible to improve processing accuracy [26] because the phase errors and random noises increase significantly in regions with dense fringes. The PSD and PDV in Figs. 1(c) and 1(f) were calculated and the results are shown in Fig. 2, with $k = 7$ in the calculations. From Fig. 2, we find that the PSD and PDV values increase significantly in regions with dense fringes (the top left corner and bottom right corner), indicating that the proposed phase retrieval method has larger PSD and PDV values and better phase performance.

Quality guide phase unwrapping (QGPU) methods are powerful noise-immune algorithms for the correct phase unwrapping of noisy phase maps [31]. An existing QGPU method is applied to prove the correctness of the proposed phase retrieval method, and the results are shown in Fig. 3. For a fair comparison,

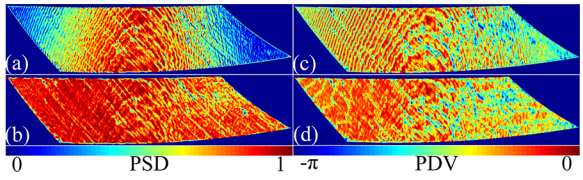

Fig. 2. Comparison of PSD and PDV: (a) PSD of traditional method; (b) PSD of proposed method; (c) PDV of traditional method; (d) PDV of proposed method.

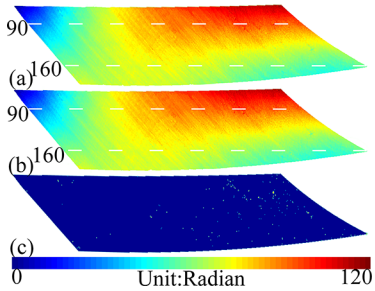

Fig. 3. Phase unwrapping results: (a) traditional method; (b) proposed method; (c) difference between the traditional and proposed methods.

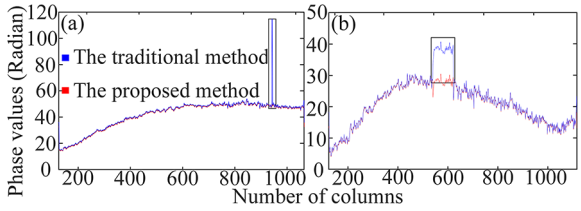

Fig. 4. Phase unwrapping results (discontinuities are in the black rectangular regions): (a) row 90; (b) row 160.

the corresponding simulation phase value is subtracted from the result of the traditional method. Figure 3(a) shows the unwrapped phase values obtained by the traditional method. Figure 3(b) shows the unwrapped phase values obtained by the proposed method. Figure 3(c) shows the difference between the two methods. The values in Fig. 3(c) are almost all zero, indicating that the results of the two methods are consistent, which proves the correctness of the proposed method.

In order to more clearly compare the proposed method and the traditional method, the unwrapped phases of rows 90 and 160 in Figs. 3(a) and 3(b) were chosen, and the results are shown in Fig. 4. The blue curve represents the results of the traditional method and the red curve represents the results of the proposed method, respectively. Figure 4 shows that the traditional method has discontinuities (the black rectangular regions), but the phase continuity of the proposed method is obviously better. The residues are an important evaluation indicator in branch-cut phase unwrapping (BCPU) and QGPU. The residues of the unwrapped phases from Figs. 1(c) and 1(f) were calculated, and the results are shown in Fig. 5. Figure 5 shows that the number of residues in the proposed method is obviously less than that in the traditional method, and that QGPU is better than BCPU in this experiment. Although the same unwrapping method is used, the proposed algorithm can reduce the discontinuities. This proves that the proposed phase retrieval method has better accuracy. Moreover, the phase values obtained by the proposed method

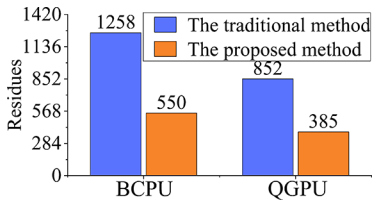

Fig. 5. Residues of the branch cut phase unwrapping (BCPU) and the quality guide phase unwrapping (QGPU).

are just the form error of the measured surface, which surely simplifies the calculation process.

This Letter proposes a phase retrieval method for phase-shifting interferometry. Different from other algorithms, the proposed method reduces the fringe density of the wrapped phase map and the difficulty of phase unwrapping, improving the phase retrieval accuracy. Moreover, the interferogram's processing flow is simplified by using the proposed method in the relevant comparative measurement processes which use the simulated phases as measurement data. This research indicates that the simulated wrapped phase can optimize phase retrieval in phase-shifting interferometry.

Furthermore, the layout of all interferometric systems, the parameters of optical components, and the model of the measured object are known. The simulated wrapped phases can be obtained, and the method proposed in this Letter can be used as a reference for phase retrieval.

The proposed method also has limitations; for instance, the measured surface is discontinuous so the phase change of its interferogram is more abrupt, and there are situations where simulated phases cannot be obtained.

Funding. National Natural Science Foundation of China (12174301, 51905412, 52205067, 91736104); The Key Laboratory of Expressway Construction Machinery of Shaanxi Province (300102250506); Natural Science Basic Research Plan in Shaanxi Province of China (2022JM-219, 2022JQ-403).

Disclosures. The authors declare no conflicts of interest.

Data availability. Data underlying the results presented in this paper are not publicly available at this time but may be obtained from the authors upon reasonable request.

REFERENCES

1. S. Yang and G. Zhang, Meas. Sci. Technol. **29**, 102001 (2018).
2. Y. Wang, F. Xie, S. Ma, and L. Dong, Opt. Lasers Eng. **93**, 164 (2017).
3. A. J. H. Meskers, J. W. Spronck, and R. H. Munnig Schmidt, Opt. Lett. **39**, 1949 (2014).
4. C. P. Chang, P. C. Tung, L. H. Shyu, Y. C. Wang, and E. Manske, Measurement **46**, 4094 (2013).
5. Y. Wu, L. Ding, and X. Hu, Opt. Commun. **284**, 1496 (2011).
6. Z. Tian, W. Yang, Y. Sui, Y. Kang, W. Liu, and H. Yang, Opt. Express **20**, 10761 (2012).
7. S. P. Fang, X. D. Zhu, P. C. Yang, Q. W. Cai, M. Komori, and A. Kubo, Opt. Eng. **53**, 084111 (2014).
8. S. Fang, L. Wang, P. Yang, L. Meng, M. Komori, and A. Kubo, J. Opt. Soc. Am. A **28**, 590 (2011).
9. S. Zhang, Opt. Lasers Eng. **107**, 28 (2018).
10. N. Wang, J. Ma, H. Ding, C. Wei, X. Miao, Z. Shen, and C. Yuan, Opt. Lett. **47**, 4371 (2022).
11. H. Zhong, J. Tang, S. Zhang, and X. Zhang, IEEE Geosci. Remote Sensing Lett. **11**, 215 (2014).
12. S. Fang, L. Meng, L. Wang, P. Yang, and M. Komori, Appl. Opt. **50**, 5446 (2011).
13. M. Zhao, L. Huang, Q. Zhang, X. Su, A. Asundi, and Q. Kemao, Appl. Opt. **50**, 6214 (2011).
14. B. Li, C. Tang, Q. Zhou, and Z. Lei, Appl. Opt. **58**, 219 (2019).
15. X. Wang, S. Fang, and X. Zhu, Appl. Opt. **56**, 4543 (2017).
16. G. H. Kaufmann, G. E. Galizzi, and P. D. Ruiz, Appl. Opt. **37**, 3076 (1998).
17. C. Wei, J. Ma, X. Miao, N. Wang, Y. Zong, and C. Yuan, Opt. Express **30**, 1686 (2022).
18. X. Xie, Opt. Express **24**, 18872 (2016).
19. X. Xie and G. Dai, Appl. Opt. **56**, 9423 (2017).
20. X. Xie and J. Li, Appl. Opt. **61**, 6677 (2022).
21. Z. Cheng, D. Liu, Y. Yang, T. Ling, X. Chen, L. Zhang, J. Bai, Y. Shen, L. Miao, and W. Huang, Opt. Express **23**, 32337 (2015).
22. Y. Qin, S. Wan, Y. Wan, J. Weng, W. Liu, and Q. Gong, Appl. Opt. **59**, 7258 (2020).
23. X. Xie, X. Tian, Z. Shou, Q. Zeng, G. Wang, Q. Huang, M. Qin, and X. Gao, Appl. Opt. **61**, 6861 (2022).
24. T. Zhang, S. Jiang, Z. Zhao, K. Dixit, X. Zhou, J. Hou, Y. Zhang, and C. Yan, Opt. Express **27**, 23173 (2019).
25. K. Wang, Y. Li, Q. Kemao, J. Di, and J. Zhao, Opt. Express **27**, 15100 (2019).
26. S. Fang, X. Zhu, P. Yang, Q. Cai, M. Komori, and A. Kubo, Opt. Commun. **328**, 49 (2014).
27. X. Zhu, S. Fang, P. Yang, X. Wang, and M. Komori, Opt. Eng. **57**, 094102 (2018).
28. S. Fang, L. Wang, M. Komori, and A. Kubo, Appl. Opt. **49**, 6409 (2010).
29. S. Fang, L. Wang, S. Liu, M. Komori, and A. Kubo, Opt. Eng. **50**, 055601 (2011).
30. X. D. Zhu, Z. H. Wang, P. C. Yang, P. Zhang, X. Wang, Z. D. Zhao, J. L. Meng, and X. Wei, Meas. Sci. Technol. **33**, 105006 (2022).
31. J. M. Bioucas-Dias and G. Valadao, IEEE Trans. on Image Process. **16**, 698 (2007).